Precision Enhancement of CAR-NK Cells through Non-Viral Engineering and Highly Multiplexed Base Editing

Minjing Wang[1,2,3,4], Joshua B. Krueger[1,2,3], Alexandria K. Gilkey[1,2,3], Erin M. Stelljes[1,2,3], Mitchell G. Kluesner[1,2,3,5], Emily J. Pomeroy[1,2,3], Joseph G. Skeate[1,2,3], Nicholas J. Slipek[1,2,3], Walker S. Lahr[1,2,3], Patricia N. Claudio Vázquez[1,2,3,4], Yueting Zhao[1,2,3], Ella J. Eaton[1,2,3,4], Kanut Laoharawee[1,2,3,4], Beau R. Webber[1,2,3], Branden S. Moriarity[1,2,3]

1 Department of Pediatrics, University of Minnesota, Minneapolis, MN, USA.

2 Masonic Cancer Center, University of Minnesota, Minneapolis, MN, USA.

3 Center for Genome Engineering, University of Minnesota, Minneapolis, MN, USA.

4 Department of Genetics, Cell Biology and Development, University of Minnesota, Minneapolis, MN, USA.

5 Molecular and Cellular Biology Graduate Program, Fred Hutchinson Cancer Center, Seattle, WA, USA.

13   **Abstract**

14   Natural killer (NK) cells' unique ability to kill transformed cells expressing stress ligands or

15   lacking major histocompatibility complexes (MHC) has prompted their development for

16   immunotherapy. However, NK cells have demonstrated only moderate responses against cancer

17   in clinical trials and likely require advanced genome engineering to reach their full potential as a

18   cancer therapeutic. Multiplex genome editing with CRISPR/Cas9 base editors (BE) has been used

19   to enhance T cell function and has already entered clinical trials but has not been reported in human

20   NK cells. Here, we report the first application of BE in primary NK cells to achieve both loss-of-

21   function and gain-of-function mutations. We observed highly efficient single and multiplex base

22   editing, resulting in significantly enhanced NK cell function. Next, we combined multiplex BE

23   with non-viral *TcBuster* transposon-based integration to generate IL-15 armored CD19 CAR-NK

24   cells with significantly improved functionality in a highly suppressive model of Burkitt's

25   lymphoma both *in vitro* and *in vivo*. The use of concomitant non-viral transposon engineering

26   with multiplex base editing thus represents a highly versatile and efficient platform to generate

27   CAR-NK products for cell-based immunotherapy and affords the flexibility to tailor multiple gene

28   edits to maximize the effectiveness of the therapy for the cancer type being treated.

Introduction

Natural killer (NK) cells have garnered extensive attention in immunotherapy due to their unique ability to kill transformed cells lacking major histocompatibility complexes (MHC) and antibody bound target cells through antigen-dependent cellular cytotoxicity (ADCC). From simply infusing allogeneic donor NK cells for treating hematological malignancies[1] to adoptive therapy harnessing NK cells with chimeric antigen receptor (CAR) for a wide range of solid tumors, NK cells have exhibited many advantages over T cell-based therapy[2]. Despite promising early outcomes in clinical studies, rarely have NK cell therapies led to durable complete remission or tumor clearance[3,4]. Extensive studies have pointed to NK cell dysfunction, exhaustion, and lack of persistence as major contributing factors to the modest clinical outcomes[5].

To date, engineering NK cells to express CAR constructs has relied almost exclusively on viral transduction with retroviruses[6]. Although highly efficient at delivering CAR constructs into NK cells, retrovirus cargo size limits and the risk of insertional oncogenesis present major drawbacks for clinical applications[6]. Comparatively, DNA transposon systems are less restricted by cargo size and afford a more economical and expeditious path to clinical manufacturing of CAR-NK cells[7]. Moreover, transposon systems allow for stable gene transfer in NK cells, which has distinct advantages over other non-viral systems, such as transient mRNA transfection[6].

Limited *in vivo* persistence and durability issues in the absence of cytokine support are major challenges to effective NK-based immunotherapy[8]. Notably, NK cell persistence, metabolic fitness, and functionality have been enhanced through supplementation with exogenous IL-15 or IL-2 *in vitro* and *in vivo*[9–14], suggesting gamma chain cytokine support may be a prerequisite to

52 successful NK-based immunotherapies[8,15]. To this end, some NK-based clinical trials tested

53 continuous intravenous infusion (CIV) of IL-15 to maintain NK cell persistence; however, this

54 costly and toxic approach has driven researchers to develop IL-15 expressing NK cells, i.e.

55 cytokine armored NK cells[15–18]. In fact, recent preclinical and clinical studies have demonstrated

56 successful expression of soluble IL-15 (sIL-15) in CAR-NK cells using retroviral engineering,

57 which led to improved cytotoxicity and persistence *in vivo*[17–19].

58

59 Beyond cytokine armoring, we[20] and others[21–24] have demonstrated that CRISPR/Cas9 can be

60 utilized to enhance NK cell function through targeted gene knockout (KO). However, this

61 approach is not ideal for multiplex gene KO as translocations and other genomic rearrangements

62 can occur due to simultaneous induction of multiple double strand breaks (DSBs). Due to these

63 concerns, we previously deployed base editor technology in primary human T cells to enhance

64 CAR-T cell function through multiplex gene KO[25]. Base editors consist of a catalytically inactive

65 Cas9 fused to a deaminase domain for site specific nucleotide base conversion, allowing users to

66 install gain or loss of function mutations without induction of a DSB or requirement for a DNA

67 donor molecule[26–29]. However, BEs have yet to be deployed for primary NK cell engineering to

68 achieve similar multiplex base editing.

69

70 Here, we report the first highly efficient engineering of NK cells using an adenine base editor

71 (ABE), ABE8e[30], to achieve both loss-of-function and gain-of-function mutations in NK cells to

72 improve their function. We also explored the upper limit of simultaneous multiplex base editing

73 and observed no significant reduction in base editing efficiency targeting up to 6 independent loci.

74 Next, we identified optimal, synergistic multiplex KO combinations and co-delivered a CD19

75   CAR and IL-15 armoring using the *TcBuster* DNA transposon system to develop a non-viral

76   engineered CAR-NK cell product tailored specifically to overcome a highly suppressive model of

77   Burkitt's lymphoma. Our work serves as a proof of concept that precision enhancement of CAR-

78   NK cells can be achieved using simultaneous multiplex base editing and non-viral transposon-

79   based engineering to generate CAR-NK therapies tailored for user defined cancer types.

80

81 **Results**

82 **Highly efficient single gene KO in primary human NK cells using ABE**

83 Base editors (BEs) are capable of highly efficient gene KO without double-stranded break

84 induction through splice site disruption or installations of stop codons[25,31–35]. We first examined

85 whether single gene KO could be achieved using BE in primary NK cells and evaluated consequent

86 changes in immune function. Given that suppression of inhibitory signals is one of the most

87 common strategies for enhancing NK-based therapy[36], we assembled a panel of targets focusing

88 largely on intracellular and extracellular inhibitory proteins expressed by NK cells **(Table 1)**.

89 Intracellular checkpoints include AHR, a negative regulator of NK cell cytotoxicity when agonists

90 (i.e. kynurenine) are present in the tumor microenvironment (TME)[37], and cytokine-inducible

91 SH2-containing protein (CISH), a negative regulator of IL-15 signaling essential for NK cell

92 development and function[34]. On the surface of NK cells, programmed cell death protein 1

93 (*PDCD1*) and T-cell immunoreceptor with Ig and ITIM domains (*TIGIT*) are well-defined

94 inhibitory immune checkpoints whose signal blockade has been seen a wide range of clinical

95 applications[38,39]. KLRG1, an emerging target in immunotherapy, is an additional inhibitory

96 immune checkpoint with potential clinical relevance[40]. Since our previous BE studies found

97 targeting splice-donors (SD) is the most efficient method for gene disruption, we designed sgRNAs

98 targeting a SD in each gene of interest using SpliceR, an in-house-developed online BE sgRNA

99 design and prediction tool[35]. Each sgRNA was co-transfected with ABE8e mRNA into feeder-

100 stimulated peripheral blood (PB) NK cells isolated from healthy donors by electroporation. KO

101 efficiency was then assessed at the genomic level through Sanger sequencing and quantification

102 of A to G conversion rates using EditR software **(Figure 1a)**[41]. Specifically, A to G conversion

103   rates for each targeted gene were as follows: *AHR* 100% (± 0%), *CISH* 99.67% (± 0.58%), *KLRG1*

104   65.07% (± 14.86%), *TIGIT* 100% (± 0%), *PDCD1* 86.33% (± 7.51%). Example sequencing results

105   of each target gene as assessed by EditR are shown in **Supplement Figure 1a-e**[41]. Of note, indels

106   were not detectable for any of the target genes in all 3 donors **(Supplement Figure 2)**. Next, we

107   assessed protein level KO of each target gene via western blot (WB) or flow cytometry using

108   donor-matched control NK cells **(Figure 1b & Supplement Figure 3a-d)**. For intracellular

109   proteins, WB analysis showed an average protein reduction of 95.60% (± 3.88%) for AhR, and

110   99.59% (± 0.71%) for CIS. Flow analysis demonstrated a 96.78% (± 4.41%) reduction of TIGIT

111   surface expression, while KLRG1 showed an average of 65% (± 14.86%) reduction in protein

112   expression. Note that PD-1 protein loss results are not shown here, as minimal detection of PD-1

113   was achieved in all healthy donors used. This observation is in line with previous studies reporting

114   low *detectable* expression (<5%) of PD-1 in NK cells of healthy individuals and elevated

115   expression in patients bearing tumors[42–50].

116

117   We next assessed whether individual gene KOs translated into the expected functional

118   enhancement of NK cells by designing functional assays specific for each gene target. Starting

119   with the intracellular targets, AHR agonists are known to suppress NK cell cytotoxicity during

120   tumor progression and metastasis[37,51]. Thus, we cultured NK cells with an AHR agonist, L-

121   Kynurenine (L-Kyn), for two rounds of 7-day expansion (14 days) before co-culturing them with

122   K562 target cells at various effector to target (E:T) ratios **(Figure 1c)**. Our results showed that L-

123   Kyn significantly reduced NK cell killing overall, however, *AHR* KO NK exhibited significantly

124   higher levels of killing than control NK **(Figure 1d & e and Supplement Figure 4a-d)**. Due to

125   its role in negative regulation of IL-15 signaling, several groups reported improved functionality

126   of NK cells with *CISH* KO[34,52,53]. Here, we co-cultured *CISH* KO and control NK cells with an

127   aggressive acute myeloid leukemia (AML) cell line, Molm-13, for 48 hours at multiple E:T ratios

128   **(Figure 1f)**. Compared to control NK, *CISH* KO NK exhibited enhanced cytotoxicity against

129   Molm-13 cells, in line with previous reports **(Figure 1g)**[34,52,53].

130

131   Next, we examined the functional impacts of surface checkpoint KOs. TIGIT/CD155 interaction

132   serves as an inhibitory immune checkpoint in NK cells, and other studies have demonstrated

133   enhanced NK cell cytotoxicity with *TIGIT* KO[54–56]. In line with these reports, BE mediated *TIGIT*

134   KO NK cells co-cultured with Raji cells engineered to overexpress CD155 (i.e. Raji CD155^{hi} cells)

135   for 48 hours at different E:T ratios exhibited significantly higher cytotoxicity against Raji CD155^{hi}

136   cells compared to donor-matched control NK cells **(Figure 1h, i)**. Analogous to TIGIT/CD155,

137   the PD-1/PD-L1 axis is another well-known inhibitory immune checkpoint in NK cells[57–60]. BE

138   mediated *PDCD1* KO NK cells co-cultured with Raji cells engineered to overexpress express PD-

139   L1 (i.e. PD-L1^{hi} cells) showed enhanced killing versus control NK cells **(Figure 1j, k)**. Finally, E-

140   cadherin (E-Cad) binding to KLRG1 has been shown to protect tumor cells from cytolysis by NK

141   cells[61]. Thus, we co-cultured NK cells with either E-Cad(+) cells (Raji) or E-Cad(-) cells (Jurkat)

142   and performed intracellular cytokine staining (ICS) to assess activation **(Figure 1l)**. In contrast to

143   previous reports, we observed no significant differences in CD107a positivity and interferon-

144   gamma (IFN-γ) expression between control NK and KLRG1 KO NK against E-Cad(+) or E-Cad(-)

145   target cells **(Figure 1m, n)**. In summary, using ABE8e we were able to achieve highly efficient

146   single gene KO in NK cells, which translated into *in vitro* functional enhancement against multiple

147   tumor   models,   with   the   exception   of   *KLRG1*   KO.

148

Highly efficient installation of a non-cleavable CD16A mutation in NK cells using ABE

Given that BE can target individual nucleotides to alter amino acid codons, we next sought to establish whether ABE could be used to enhance NK cell function through gain-of-function mutations. CD16a is an Fc receptor expressed on the surface of NK cells which mediates antibody-dependent cell-mediated cytotoxicity (ADCC)[62]. Upon NK cell activation, CD16a undergoes a proteolytic cleavage process by ADAM17 as a negative feedback mechanism regulating NK cell cytotoxicity **(Figure 2a)**[63]. Previous studies have found that a single amino acid substitution (S197P) at the cleavage site of ADAM17 on CD16a rendered the receptor "non-cleavable", and expression of the non-cleavable CD16a (ncCD16a) cDNA in NK cells enhanced ADCC[64]. Here, we sought to install the non-cleavable CD16a (ncCD16a) mutation at the endogenous locus using ABE8e as a proof-of-principle of ABE-based gain-of-function engineering in NK cells. To this end, we designed a sgRNA targeting serine197 at the ADAM17 cleavage site with the goal of replicating the S197P mutation through a single A to G base conversion, altering the mRNA codon from UCA to CCA **(Figure 2b)**. Sequencing results validated our prediction and yielded an average A to G conversion rate of 89% (± 9.17%, n=3) in NK cells with the highest conversion rate observed at 99% in one donor **(Figure 2c; Supplement Figure 5a)**. To assess whether the installation of this mutation conferred cleavage resistance, NK cells were stimulated with phorbol 12-myristate 13-acetate (PMA) to activate ADAM17 and then assessed for CD16a retention (i.e. % of CD16a detected with PMA treatment versus % of CD16a detected without PMA treatment). As shown in **Figure 2d & Supplement Figure 5b**, we observed an average of 97.17% (± 2.45%)

169   CD16a retention after PMA treatment in ABE8e engineered NK cells, with the highest retention

170   rate approaching 100%.

171

172   Next, to validate the functionality of our ncCD16a NK cells, we tested their ability to mediate

173   ADCC against Raji cells treated with an anti-hCD20-mAb. We first assessed activation of

174   ncCD16a NK cells in this assay via ICS for degranulation (CD107a) and cytokine production

175   (TNF-α and IFN-γ). Compared to non-engineered NK cells, ncCD16a NK cells demonstrated

176   significantly increased CD107a, IFN-γ, and TNF-α expression when co-cultured with cell targets

177   treated with anti-hCD20-mAb, indicating enhanced ADCC-driven activation (measured by Raji

178   versus Raji co-treatment with anti-hCD20-mAb) of ncCD16a NK cells **(Figure 2e)**. Functionally,

179   we assessed NK cytotoxicity via ADCC using an ADCC co-culture killing assay against Raji cells

180   at different E:T ratios. As predicted, ncCD16a NK exhibited significantly enhanced killing of Raji

181   cells compared to control NK cells throughout all E:T ratios tested **(Figure 2f)**. Surprisingly, when

182   co-cultured without anti-hCD20-mAb, ncCD16a NK also demonstrated significantly enhanced

183   killing compared to that of control NK cells **(Supplement Figure 5c)**. Taken together, these data

184   demonstrate that ABE is capable of installing gain-of-function mutations in NK cells at high

185   efficiencies to improve NK cell functionality.

186

187   **Highly efficient multiplex base editing in NK cells using ABE.**

188   Next generation cellular therapies will likely require a multitude of tailored gene edits to maximize

189   efficiency, particularly when addressing hard to treat solid tumor cancers. Previously, our group

190   has shown multiplex base editing can be used to enhance CAR-T cell function[25]. Here, we

191   examined whether the same approach can be applied in developing NK-based cell therapies using

192   ABE8e and also attempted to find the upper limits of multiplex base editing. We started with one

193   sgRNA targeting *TIGIT* and subsequently added sgRNAs one at a time in the following order:

194   ncCD16a sgRNA, AHR sgRNA, KLRG1 sgRNA, CISH sgRNA, PDCD1 sgRNA up to a total of

195   6 sgRNAs **(Figure 3a)**. Multiplex editing efficiencies at the genomic level were again assessed

196   via Sanger sequencing of A to G conversions at target sites assessed using EditR. Impressively,

197   we observed no significant loss of editing efficiency at any loci using up to 6 sgRNAs

198   simultaneously **(Figure 3b and Supplement Figure 6a-f)**. Editing efficiencies at protein level,

199   measured by protein loss (for AhR, CISH, KLRG1, TIGIT, and PD-1) or CD16a retention rate

200   after PMA treatment were consistent with genomic base editing levels **(Figure 3c and**

201   **Supplement Figure 7a-e)**. In summary, these data demonstrate that highly efficient multiplex

202   base editing is achievable in NK cells using ABE and the upper limit of simultaneous base edits

203   has   not   yet   been   reached   in   this   context.

204

205   **Tailored multiplex engineering of NK cells for optimized cytotoxicity against Raji**

206   **CD155^hi/PD-L1^hi cells**

207   In order to demonstrate a tailored editing approach for NK based cancer immunotherapy, we next

208   sought to determine an optimal combination of multiplex edits that yields the most potent NK cell

209   cytotoxicity for a chosen tumor model. Two of the most common factors leading to poor prognosis

210   in many cancers are high expression of PD-L1 and CD155[65–73]. To model this, we generated a Raji

211   cell line that over-expresses both checkpoint ligands (i.e. Raji^hi/hi) **(Supplement Figure 8)**. To

212   determine the optimal multiplex base editing combination, we started with TIGIT (CD155 ligand)

213   and PDCD1 (PD-L1 ligand) KO to avoid suppression from CD155 and PD1, respectively. Next,

214   these edits were combined with AHR KO, CISH KO, or both KOs for testing different base editing

215   combinations **(Figure 4a)**. Editing efficiencies showed the average A to G conversions of each

216   target site in all combinations were above 90%, and similar results were observed for average

217   protein loss of all KOs **(Figure 4b, c)**. In order to assess the functional consequences of the various

218   combinations of base edits, we first performed co-culture killing assays with Raji[hi/hi] cells at

219   different E:T ratios. We observed that unedited NK cells had the lowest level of killing against

220   Raji[hi/hi] and there was no significant difference in killing between TIGIT+PDCD1 (TP) KO NK,

221   TIGIT+PDCD1+AHR (TPA) KO NK, and TIGIT+PDCD1+AHR+CISH (TPAC) KO NK.

222   However, knocking out TIGIT, PDCD1, and CISH (TPC) demonstrated the highest killing against

223   Raji[hi/hi] cells compared to all other combinations **(Figure 4d-e and Supplement Figure 9a-d)**.

224   These data demonstrate that TPC KO NK cells have the most robust cytotoxicity against Raji[hi/hi]

225   cells   compared   to   all   other   multiplex   base   editing   combinations.

226

227   **Simultaneous multiplex base editing and non-viral transposon engineering generates highly**

228   **functional CAR-NK cells**

229   Chimeric antigen receptors (CARs) have emerged as one of the most promising tools for enhancing

230   cell-based cancer immunotherapy in the past decade[74]. To date, delivery of CAR constructs into

231   NK cells has been largely limited to the use of viral vectors[75–77]. The cost and extended

232   manufacturing process of viral vectors drives the needs for a faster and more economical

233   alternative method for stable transgene delivery. Thus, to develop an effective non-viral

234   engineered CAR-NK cell product, we designed a *TcBuster* transposon plasmid encoding a CD19

235   CAR **(Figure 5a; 'CAR').** In an effort to test whether cytokine armoring of CAR-NKs would

236   enhance persistence and activity, we designed an additional transposon plasmid encoding sIL15

237   **(Figure 5a; 'CAR15')**. Notably, IL15 has been shown to be necessary to support NK cell

238   persistence in NOD-scid IL2R gamma-null (NSG) models[78,79]. Each transposon contains the MND

239   promoter, 2nd generation CD19-targeting CAR, and RQR8 **(Figure 5a)**. RQR8 is a synthetic cell

240   surface receptor with CD34 and CD20 epitopes and was included here for flow cytometry

241   detection and immunomagnetic enrichment of CAR-expressing NK cells[80].

242

243   For engineering, NK cells were feeder expanded before co-delivery of CD19 CAR transposon

244   plasmid, *TcBuster* transposase mRNA, sgRNAs, and ABE8e mRNA through electroporation

245   **(Figure 5b)**. Following a subsequent 7-day NK cell feeder expansion, CD19 CAR integration rate

246   was assessed via flow cytometry before CAR enrichment through RQR8 immunomagnetic

247   selection **(Figure 5c)**. CAR integration rates in each group were reasonably efficient in multiple

248   donors (57.4%-81.3% for CAR and 20.1%-39.9% for CAR15) and comparable to previously

249   reported integration rates of CD19 CAR through retroviral transduction[75,77]. We also assessed the

250   insertion site profile of *TcBuster* transposons and found that it integrated in coding genes less

251   frequently than lentivirus or retrovirus regardless of construct **(Supplement Figure 10a)**.

252   Additionally, evaluation of the distance between integration events and transcriptional start sites

253   indicated that *TcBuster* integrated further away from transcriptional start sites when compared to

254   lentivirus and retrovirus **(Supplement Figure 10b)**. CAR enrichment was further performed to

255   ensure CAR-expression across groups was not significantly different, which could confound

256   results comparing across groups. After a third and final feeder-based expansion, CD19 CAR

257   expression was assessed by flow cytometry **(Figure 5c)** and IL-15 expression was confirmed

258   through ELISA **(Supplement Figure 11;** CAR15: 220.0 ± 5.09 pg/mL, CAR15/TPC^{KO}: 340.9 ±

259   20.34 pg/mL). Control groups lacking transposon engineering demonstrated base editing levels

260   comparable to previous results in TPC KO NK cells **(Figure 4b)**, while a 10-25% reduction in

261   base editing efficiency was observed in groups with transposon co-delivery **(Figure 5d)**. However,

262   the average protein reduction of each gene of interest in all KO groups was above 90%, with one

263   outlier NK donor from the CAR15/TPC^{KO} group having lower TIGIT protein reduction **(Figure**

264   **5e)**.

265

266   The functionality of all engineered NK cell groups was first assessed using co-culture killing

267   assays with Raji$^{hi/hi}$ cells at a range of E:T ratios. We observed no significant differences in killing

268   between CAR and CAR15 groups, but a moderate enhancement of killing by CAR15/TPC^{KO} group

269   compared to CAR/TPC^{KO} NK cells **(Figure 5f-g and Supplement Figure 12a-d)**. TPC^{KO} also

270   improved cytotoxicity of NK cells, with both CAR/TPC^{KO} and CAR15/TPC^{KO} groups exhibiting

271   better killing against Raji$^{hi/hi}$ cells when compared to that of their corresponding CD19 CAR only

272   groups. These data demonstrate that CAR15/TPC^{KO} NK cells exhibited the most significant

273   functionality improvement against Raji$^{hi/hi}$ targets *in vitro*.

274

275   **Multiplex base edited CD19 CAR-NK cells are highly functional *in vivo***

276   To test the efficacy of our multiplex base edited CAR-NK cell product *in vivo*, we used Raji$^{hi/hi}$

277   cells as a highly suppressive xenograft model of Burkitt's lymphoma. NSG mice were xenografted

278   with 1E5 of Raji$^{hi/hi}$ through intravenous injection (I.V.) on day 0, followed by a randomization

279   into treatment groups of equivalent tumor burden prior to therapy delivery **(Supplement Figure**

280   **13a)**. Mice receiving therapy were dosed with two rounds of engineered NK cells 14 days apart

281   (day 3 and 17) **(Figure 6a)**. Mouse body weight and bioluminescent imaging (BLI) of tumor

282   burden were monitored weekly until predefined humane endpoints were reached **(Figure 6b and**

283   **Supplement Figure 13b)**. Bioluminescent imaging results suggested tumor progression was

284   significantly delayed in groups treated with CAR15 NK (n=5) and CAR15/TPC^{KO} NK (n=5)

285   compared to all other groups **(Figure 6b, c)**. Mouse tumor burden of these two groups was

286   significantly reduced by day 23, the last imaging time point before mice began to meet endpoint

287   criteria **(Figure 6d)**. The survival of mice receiving CAR15 and CAR15/TPC^{KO} NK was

288   significantly improved compared to control NK treated animals (median survival in days: CAR15

289   vs Ctrl 63 vs 25, p<0.01; CAR15/TPC^{KO} vs Ctrl 30 vs 25, p<0.05); however, in contrast to the *in*

290   *vitro* killing assays, we saw no significant differences between CAR15 NK and CAR15/TPC^{KO}

291   NK (median survival in days: CAR15 vs CAR15/TPC^{KO} 63 vs 30, p=0.5982) **(Figure 6e)**. Among

292   all 5 mice in the CAR15 group, four animals were euthanized due to paralysis and one animal due

293   to rapid loss of body weight. Necropsy of the animal with rapid weight loss revealed a significantly

294   enlarged ovary on the left side **(Supplement Figure 13c)**. For the CAR15/TPC^{KO} group, one

295   animal survived long term (128 days) before presenting with paralysis, two animals were

296   euthanized due to rapid body weight loss and were found to harbor enlarged ovaries and/or brain

297   tumor masses. Two CAR15/TPC^{KO} treated animals were also euthanized due to rapid body weight

298   loss with no significant tumor burden detected **(Figure 6b, Supplement Figure 13c)**. Histology

299   of ovary and brain tumors indicated a domination of hCD19+ cells with no signs of hCD56+ NK

300   cells **(Supplement Figure 13d)**.

301

302   Weekly peripheral blood (PB) collection and endpoint PB, bone marrow (BM) and spleen

303   collections were performed to monitor the persistence of NK cells in each treatment group **(Figure**

304   **6f, Supplement Figure 13e, g&h)**. We observed a significantly higher level of NK cells in blood,

305   BM and spleen at endpoint in CAR15/TPC^{KO} NK group than any other groups **(Figure 6f,**

306   **Supplement Figure 13g, h)**. Interestingly, the CAR15 group had no detectable NK cells in the

307   BM or spleen and minimal NK cells in PB. **(Figure 6f, Supplement Figure 12g, h)**. The amount

308   of Raji$^{hi/hi}$ cell in BM was also determined at endpoint, where we observed a significantly lower

309   frequency of Raji$^{hi/hi}$ cells in CAR15 NK and CAR15/TPC^{KO} NK groups compared to other groups,

310   yet no significant difference was observed between the two groups **(Supplement Figure 12j)**.

311   Together, we observed a significant improvement in tumor control and overall survival of mice

312   treated with NK cells expressing sIL-15, with the CAR15/TPC^{KO} NK group exhibiting a slightly

313   improved persistence but no survival advantages over CAR15 NK.

Discussion

Cellular therapy using CAR-expressing primary effector cells has shown great success in the clinic and resulted in multiple FDA-approved treatments for hematologic malignancies and solid tumors[2]. These current-generation of FDA-approved CAR therapies largely utilize autologous α/β T cell chassis and viral vector engineering methods, which limits the scope of potential therapy recipients and results in high manufacturing costs and long timelines. A more appealing approach is to utilize a universal cell type, such as primary NK cells, that are engineered using non-viral methods. Further, as the landscape of cancer therapy shifts towards solid tumors, it is increasingly evident that methods such as cytokine armoring and immune checkpoint editing through genome engineering will be required to create more potent and persistent therapies. Since CRISPR/Cas9 was co-opted for genome editing over a decade ago, engineering efficiencies in primary immune cells have been significantly improved[81,82]. It remains, however, that indels and translocations caused by Cas9 induced DSBs could negatively impact cellular function and introduce major safety concerns for CRISPR/Cas9-based therapies[81,83]. In an effort to circumvent this issue, we applied base editing technology to NK cell engineering for the first time and demonstrated NK cells could be multiplex engineered with undetectable rates of insertions or deletions (indels). KO of our selected targets or installation of gain of function edits resulted in increased baseline functionality, which could be combined to further increase performance. We then combined multiplex base editing with non-viral transposon engineering to generate a CAR-NK engineering pipeline for precision enhancement of next generation CAR-NK cell products. These multiplex base-edited CAR-NK cells showed improved functionality *in vitro* and *in vivo* against a

335   challenging model of Burkitt's lymphoma model and provide compelling pre-clinical evidence for

336   a future NK based CAR therapy option.

337

338   Our initial engineering studies examined whether NK cells were amenable to individual targeted

339   base editing at high-frequency and how these edits impact NK cell function. We began with

340   selecting a variety of targets that play inhibitory but critical roles in NK cell function with an

341   emphasis on clinical relevance. To confirm that successful genetic modifications lead to protein

342   loss and functional enhancements, we validated protein loss and functional improvement as part

343   of the validation process, respectively. Other than *KLRG1*, all inhibitory target KOs exhibited the

344   predicted functional enhancement. *KLRG1* KO NK cells' failure to demonstrate improved function

345   is in line with some previous studies disrupting *KLRG1* in NK cells[84]. As speculated in those

346   studies, this contradictory finding may be attributed to a relatively low inhibitory potential of

347   *KLRG1* on NK cell function[84,85].

348

349   Our inability to detect PD-1 protein on the surface of NK cells is in line with numerous previous

350   reports and reflects the ongoing controversy of the role of PD-1 in NK cells[20,50,86,87]. For instance,

351   the Moretta group has published multiple studies on this issue and found that NK cells constantly

352   produce PD-1 mRNA and protein, but only rapidly externalize PD-1 protein upon activation by

353   certain stimuli[86]. Davis *et. al.* also reported minimal surface expression of PD-1 in NK cells from

354   healthy individuals[87]. Moreover, several previous studies have used functional assays with anti-

355   PD-1 agents to validate PD-1 expression on the NK cell surface, and our results here demonstrating

356   significant cytotoxicity improvement of *PDCD1* KO NK cells against *PD-L1+* target cells further

357   support the role of PDCD1 in NK cell inhibition by PD-L1[20,50].

358

359   We also demonstrate the ability to install gain-of-function mutations in NK cells using base

360   editing. The rapid downregulation of CD16a as a result of a proteolytic cleavage process upon NK

361   cell activation serves as a negative feedback mechanism for ADCC. In a tumor microenvironment

362   (TME) setting, functional inactivation of tumor associated NK cells reflects a further down-

363   regulation of CD16a that significantly compromises NK cell cytolytic function against tumor

364   cells[88,89]. BE installation of a non-cleavable CD16a improved both ADCC mediated killing and

365   cytokine production in NK cells. Notably, this BE mediated approach is likely significantly safer

366   and more physiologically relevant compared to integration of a ncCD16A cDNA expression

367   cassette using viral delivery[64]. Unexpectedly, we also observed a significant improvement in basal

368   killing of Raji cells with ncCD16A NK cells. We speculate that the constitutive expression of the

369   non-cleavable CD16a may result in low level tonic signaling, contributing to this phenomenon.

370   This phenomenon could further benefit patients with compromised NK cytolytic functions, and a

371   closer look at the downstream mechanisms of this phenomenon is warranted in future studies.

372

373   Moving forward to multiplex editing, we observed no significant reduction of editing efficiencies

374   with up to six co-delivered sgRNAs. Surprisingly, there was an improvement of *KLRG1* KO

375   efficiency at the multiplex level compared to the single-target experiments. One explanation for

376   this phenomenon is a potential 'carrier effect' linked to increasing the total amount of co-delivered

377   sgRNAs. This is similar to previous studies reporting a higher extracellular DNA concentration

378   leads to a higher amount of DNA delivered to the nucleus[90,91]. However, further investigation is

379   required to illuminate the exact mechanisms behind this observation.

380

381   To examine whether multiplex editing resulted in enhanced *in vitro* function, we developed and

382   utilized an engineered Burkitt's lymphoma cell line Raji[hi/hi] as a proof-of-principle model. We

383   hypothesized that the number of inhibitory gene KOs would positively correlate with the

384   improvement of NK cell function, and selected *AHR*, *CISH*, *TIGIT* and *PDCD1* as candidates.

385   *KLRG1* was excluded due to its failure to demonstrate functional improvement at single KO level.

386   Contrary to our hypothesis, the TPC KO group demonstrated the most significant improvement in

387   cytotoxicity against Raji[hi/hi] cells. Additionally, the fact that no significant differences in killing

388   were observed among TP, TPA, and TPAC KO groups throughout all E:T ratios is another

389   interesting finding that warrants further investigation. It is possible that Raji[hi/hi] cells produced

390   lower amounts of AhR ligand (kynurenine) than K562, leading to a less pronounced inhibitory

391   effect on NK cells. These findings suggest that the number of inhibitory gene KOs does not always

392   correlate with improved NK cell functionality, and an optimization of the KO combination is likely

393   required for precision enhancement against each unique tumor type of interest.

394

395   Finally, in an effort to test the impacts of multiplex editing on CAR-NK cell function, we co-

396   delivered a CD19 CAR with multiplex base editing using the *TcBuster* DNA transposon system.

397   Compared to traditional virus-based delivery methods, non-viral transposon systems significantly

398   reduce the manufacturing cost and timelines. Integration efficiencies of CD19 CAR constructs

399   were correlated with its cargo size, and are comparable to that of virus-based delivery methods[19,92].

400   One unexpected finding is the significantly higher CD19 CAR integration rate in the groups with

401   TPC KO. We suspect a similar carrier effect may be contributing to the higher rates; however,

402   further investigation is necessary to define the mechanism behind this observation[90,91]. Multiple

403   previous studies have reported improved *in vivo* persistence of CAR-NK cells with sIL-15

404   expression[17–19,93]. Here, we adopted this idea in an attempt to improve proliferation and prolong

405   the persistence of NK cell products *in vivo* by armoring cells with sIL-15. Our animal study clearly

406   demonstrated a strong correlation of IL-15 expression with NK cell persistence *in vivo*, which

407   translates into a significantly delayed tumor progression and improved overall survival compared

408   to groups without IL-15 expression. For groups treated with NK cells expressing sIL-15, one

409   animal from group CAR15 developed a tumor in the ovary, and two animals from group

410   CAR15/TPC[KO] developed a tumor in the ovary and/or brain. The fact that all these tumors

411   developed in known immune privileged areas serves as indirect evidence of robust tumor clearance

412   in peripheral blood and BM where full immune surveillance is expected[94]. The CAR15/TPC[KO]

413   group's failure to exhibit an improved survival over CAR15 group is unexpected based on our *in*

414   *vitro* results and thus requires closer examination. Among all 5 animals in the CAR15/TPC[KO]

415   group, two died with relatively low tumor burden but met endpoint criteria of significant decrease

416   of body weight. We initially suspected cytokine release syndrome (CRS) in these mice; however,

417   there was no significant increase in CRS related cytokines in serum at the endpoint (data not

418   shown). A closer look at the weekly NK cell density data revealed a rapid NK cell proliferation

419   after day 25 in 4 out 5 mice in CAR15/TPC[KO] group, and 3 of those mice died in the following

420   week. We suspect that this dramatic NK cell proliferation, not the absolute number of NK cells,

421   led to the observed toxicity and eventual death in those mice, as the absolute number of NK cells

422   in CAR15 group was equal to, if not higher, than that of the CAR15/TPC^{KO} group. Our observation

423   is consistent with a previous study using sIL-15 expressing CAR-NK cells, which also found

424   negative evidence of CRS and attributed the observed systemic toxicity to rapid NK cell

425   proliferation *in vivo*[93]. It is worth noting that the only mouse with full tumor clearance was treated

426   with CAR15/TPC^{KO} NK cells, suggesting a potential benefit of CAR15/TPC^{KO} over CAR15

427   treatment. However, further evaluation of the CAR15/TPC^{KO} NK treatment will be required to

428   confirm improved tumor clearance and survival benefit over CAR15 NK treatment.

429

430   In summary, we reported the first application of BE in primary NK cells, with high editing

431   efficiency for both single and multiplex editing. Moreover, with co-delivery of a mult-cistronic

432   CAR construct using a non-viral transposon system, we present a highly flexible, fully non-viral

433   engineering platform that allows precision enhancement of NK-based cell therapy against various

434   types of cancer. With our proof-of-principle model, we have generated a pipeline for developing

435   a highly customized NK product for any specific type of cancer. Moving forward, we are actively

436   exploring the application of this platform into the frontier of solid tumors, including enhancement

437   of NK cell homing to tumor sites, NK cell resistance to oxidative stress, and more.

438

Methods

Production of editing reagents

ABE8e plasmid was obtained from Addgene (https://www.addgene.org/138489/) and cloned into a pmRNA vector. ABE8e mRNA was produced by Trilink Biotechnologies. Nanoplasmids for CD19 CAR were synthesized by Aldevron.

Guide RNA design

Guide RNAs (sgRNAs) for KO were designed using the base editing splice-site disruption sgRNA design program SpliceR (https://z.umn.edu/splicer). SpliceR is written in the R statistical programming language (v. 3.4.3). Briefly, SpliceR takes a target Ensembl transcript ID, a base editor PAM variant, and a species as an input. Using the exon and intron sequences from Ensembl, the program extracts the region surrounding every splice site based on a user-specified window. The pattern of N20-NGG is then matched to the antisense strand of the extracted sequence. Matched patterns are then scored based on the position of the target motif within the predicted editing window based on previous publications. Subsequently, sgRNAs are scored based on their position within the transcript, where sgRNAs earlier in the transcript receive a higher score. sgRNA for ncCD16a was designed manually to achieve the S197P mutation.

Donor NK cell isolation

Peripheral blood mononuclear cells (PBMCs) from healthy human donors were obtained by automated leukapheresis (Memorial Blood Centers, Minneapolis, MN). CD56+CD3- NK cells were isolated from the PBMC population using the EasySep Human NK Cell Isolation Kit (STEMCELL Technologies, Cambridge, MA). NK cells were frozen at 2.5e6 or 5E6 cells/mL in CryoStor CS10 (STEMCELL Technologies, Cambridge, MA).

NK cell culture

NK cells were cultured in CTS AIM VTM (ThermoFisher, Waltham, MA) with 5% CTS Immune

cell SR (ThermoFisher, Waltham, MA), and 100 IU/mL IL-2 (PeproTech, Rocky Hill, NJ). NK

cells were activated by co-culture with X-irradiated (100 Gray) feeder cells (K562 expressing

membrane-bound IL-21 and 41BB-L) at various feeder to NK ratios (2:1 prior to electroporation,

5:1 72 hours after Neon electroporation, or 1:1 immediately after MaxCyte electroporation).

NK cell electroporation

Neon electroporation:

Feeder cell-activated NK cells were washed once with PBS (Ca^{2+} and Mg^{2+} free) and resuspended

at 3E7 cells/mL in electroporation buffer. Protector RNase inhibitor (Sigma Aldrich, St. Louis,

MO) was added to the mixture at a concentration of 0.8 U/µL and incubated for 5 minutes at room

temperature. The cell mixture was added to 1.5ug of ABE8e mRNA and 1 nmol sgRNA on ice.

This mixture was electroporated in a 10 µL tip using the Neon Transfection System

(ThermoFisher, Waltham, MA) under the following conditions: 1825 volts, pulse width of 10 ms,

2 pulses. NK cells were allowed to recover at a density of 1E6 cells/mL in antibiotic-free medium

containing 100 IU/mL IL-2 (PeproTech, Rocky Hill, NJ) for 72 hours at 37°C, before expansion

with feeder cells at a 5:1 feeder to NK ratio.

MaxCyte electroporation:

NK cells reaching 10-fold increase in cell number after feeder cell-expansion were washed once

with electroporation buffer and resuspended at 1.75E8-1.00E9 cells/mL. Protector RNase inhibitor

(Sigma Aldrich, St. Louis, MO) was added to the mixture at a concentration of 0.8 U/µL and

incubated for 5 minutes at room temperature. The cell mixture was added to 4 ug of ABE8e

483   mRNA, 5ug sgRNA, 3 μg of transposase mRNA and 5 μg transposon nanoplasmid on ice. This

484   mixture was electroporated in a R-50x3 assembly using the MaxCyte System (ThermoFisher,

485   Waltham, MA) under Expanded T Cell 4 protocol. NK cells were allowed to recover at a density

486   of 1E6 cells/mL in antibiotic-free medium for 1 hour at 37°C, before expansion with feeder cells

487   at a 1:1 feeder to NK ratio.

488   **Genomic DNA analysis**

489   NK cells were harvested 10 days after electroporation, followed by DNA isolation and PCR

490   amplification of CRISPR-targeted loci using Phire Tissue Direct PCR Master Mix kit

491   (ThermoFisher, Waltham, MA). Base editing efficiency was analyzed at the genomic level by

492   Sanger sequencing of the PCR amplicons, and subsequent analysis of the Sanger sequencing traces

493   using the web app EditR (baseeditr.com)[41].

494   **Primer and sequence**

Primer name	Primer Sequence
AHR Exon 2 Splice Donor forward	TAC CAT GCA TCA TTT CAG TG
AHR Exon 2 Splice Donor reverse	TTT CAG AGT AAA GCC AAT CC
CISH Exon 2 Splice Donor forward	AAT TAG CTG GGG TAA CCA AT
CISH Exon 2 Splice Donor reverse	CCT TCT AGA CCT CGT CCT TT
TIGIT Exon 1 Splice Donor forward	GTC TGC AAA GTC CTT CAT CT
TIGIT Exon 1 Splice Donor reverse	ATA TGG TTT TTG CCA AAC TT
KLRG1 Exon 4 Splice Donor forward	CCC AAA CAG CAG AAG AAT TA
KLRG1 Exon 4 Splice Donor reverse	TAG GAA TCC AAT GTG GAA AG

PD-1 Exon 1 Splice Donor forward	ACC CTC CCT TCA ACC TGA CC
PD-1 Exon 1 Splice Donor reverse	AAG CCA CAC AGC TCA GGG TA
CD16A S197P mutation forward	TAA AGG ATA TAC GAG ATT AA
CD16A S197P mutation reverse	AAC TGG GTA ATT TAT AAC

Antibodies and flow cytometry

The following antibodies and dyes were used: APC-, FITC-, or BV650-conjugated anti-CD56 (clone 5.1H11, BioLegend; clone REA196, Miltenyi Biotec; or clone HCD56, BioLegend), FITC-conjugated anti-CD3 (clone OKT3; BioLegend), PE/Cy7-conjugated anti-PD-1 (clone EH12.2H7; BioLegend), eFluor 450- or Alexa FluorTM 700-conjugated anti-TIGIT (clone MBSA43; eBioscience), PE/DazzleTM 594- or FITC-conjugated anti-human CD45 (clone 14C2A07, BioLegend; clone SA231A2, BioLegend), PE/Cy7 anti-human CD16 (clone 3G8, BioLegend), BV421-conjugated anti-human CD45 (clone 2D1; BioLegend), BV605-conjugated anti-mouse CD45 (clone 30-F11; BioLegend), Brilliant violet 421-conjugated anti-IFNγ (clone 4S.B3; BioLegend), Alexa FluorTM 700-conjugated anti-TNF-α (clone MAb11; BioLegend), PE-conjugated anti-CD34 (clone QBEnd-10, Invitrogen), APC-conjugated anti-PD-L1 (clone B7-H1, BioLegend), FITC-conjugated anti-CD155 (clone SKII.4, BioLegend), FITC-conjugated anti-DNAM-1 (clone 11A8, BioLegend), Brilliant violet 510-conjugated anti-CD161 (clone HP-3G10, BioLegend), PE/Cyanine7-conjugated anti-Tim3 (clone F38-2E2, BioLegend), APC-conjugated anti-NKG2D (clone 1D11, BioLegend), PE-conjugated anti-NKG2A (clone S19004C, BioLegend), Alexa FluorTM 700-conjugated anti-NKp46 (clone 9E2, BioLegend), PE/DazzleTM 594-conjugated anti-NKp30 (clone P30-15, BioLegend), FITC-conjugated anti-CD107a (clone

512   H4A3; BD Biosciences), SYTOX Blue dead cell stain (ThermoFisher), Fixable viability dye

513   eFluor 780 (eBioscience). Flow cytometry were performed on a CytoFLEX S flow cytometer

514   (Beckman Coulter) and all data were analyzed using FlowJo version 10.4 software (FlowJo LLC).

515   **Immunoblotting assay**

516   Proteins were isolated from 1E6 cells in complete RIPA buffer with protease and phosphatase

517   inhibitors (Sigma-Aldrich, St. Louis, MO). Total protein was quantified using the Pierce BCA

518   Protein Assay Kit (ThermoFisher, Waltham, MA) according to the manufacturer's protocol.

519   3μg/μL of cell lysate was run and analyzed on the Wes platform after being denatured at 95 °C for

520   5 min according to the manufacturer's protocol (ProteinSimple, San Jose, CA). Primary antibodies

521   against CISH (Cell Signaling #8731), AhR (Cell Signaling #83200) and beta-actin (Cell Signaling

522   #3700) were all used at 1:50 dilutions in kit-supplied buffer and platform-optimized secondary

523   antibodies were purchased from ProteinSimple.

524   **NK cell intracellular cytokine staining (ICS) assay**

525   Activated NK cells were plated at 1E6 cells/mL in NK cell medium without cytokines. After

526   incubation overnight, the Burkitt's Lymphoma cell line Raji or T-cell leukemia cell line Jurkat was

527   added at an effector-to-target (E:T) ratio of 1:1. FITC-conjugated anti-CD107a was added to the

528   culture and cells were incubated for 1 hour at 37ºC. Brefeldin A and monensin (BD Biosciences,

529   San Jose, CA) were added and cells were incubated for 4 hours. Cells were stained with fixable

530   viability dye, then for extracellular antigens. Cells were fixed and permeabilized using BD

531   Cytofix/Cytoperm (BD Biosciences, San Jose, CA) following manufacturer's instructions. Cells

532   were then stained for intracellular IFN-γ and/or TNF-α and analyzed by flow cytometry.

533   **NK cell cytotoxicity assays**

534   Cancer cell lines were seeded into a black round-bottom 96-well plate (5E4 cells per well). NK

535   cells were added to the wells in triplicate at the indicated E:T ratios. Target cells without effectors

536   served as a negative control (spontaneous cell death) and target cells incubated with 1% Triton X-

537   100 served as a positive control (maximum killing). Co-cultures were incubated at 37°C for 48

538   hours. After incubation, D-luciferin (potassium salt; Gold Biotechnology, St. Louis, MO) was

539   added to each well at a final concentration of 25 ug/mL and incubated for 5 minutes with gentle

540   shaking. Luminescence was read in endpoint mode using a BioTek Synergy microplate reader. For

541   *in vitro* killing assays, percent CAR expression was equalized across groups using matched NK

542   cells (for CD19 CAR only groups) or TPC^{KO} NK cells (for co-delivery groups), before co-culture

543   set up.

Antibody-dependent cellular cytotoxicity assay

545   CD20+ Raji cells were pre-treated with anti-hCD20 mAb (InvivoGen, San Diego, CA) at 10

546   μg/mL for 30 min at 37°C, washed with PBS, and seeded into a black round-bottom 96-well plate

547   (5E4 cells per well). NK cells were added to the wells in triplicate at the indicated E:T ratios. Co-

548   cultures were incubated at 37°C for 4 hours. After incubation, D-luciferin (potassium salt; Gold

549   Biotechnology, St. Louis, MO) was added to each well at a final concentration of 25 ug/mL and

550   incubated for 5 minutes with gentle shaking. Luminescence was read in endpoint mode using a

551   BioTek Synergy microplate reader.

Transposon integration sequencing

553   Genomic DNA was isolated from engineered CAR-NK cells as previously described[95]. Briefly,

554   sequencing libraries were prepared from 150 ng genomic DNA quantified by Picogreen (Life

555   Technologies) using the Lotus DNA Library Prep Kit (Integrated DNA Technologies) according

556   to the manufacturer's specifications for libraries undergoing target enrichment. Ligations used

557   vendor-supplied "stubby" adapters, with sample-specific 8-bp unique dual indices (UDIs) added

558   during final library amplification. Hybridization capture was performed per manufacturer's

559   protocol with up to 16 libraries in multiplex (500ng per library) using xGen universal blocking

560   oligos (IDT) and a custom biotinylated xGen oligo probe pool designed to hybridize to the inserted

561   transposon sequence. Given the small probe panel size, hybridizations and temperature-sensitive

562   washes were performed at 63 °C and the total hybridization time was increased from 4 h to 16 h.

563   Captured libraries were then amplified to ≥2 nM using KAPA HiFi HotStart 2X PCR master mix,

564   quantified by Picogreen, sized on an Agilent TapeStation using the D1000 assay, normalized, and

565   pooled for 150-bp paired-end sequencing on an Illumina NovaSeq* SP flowcell.

566   **Transposon integration analysis**

567   We analyzed integration site data for TcBuster and compared results to published literature data

568   for integration sites of other transposase and viral systems as previously described[95]. Specifically,

569   comparison sequencing datasets were generated by outside sources using different experimental

570   methods. Raw reads from comparison datasets were retrieved (Accession IDs: Lentivirus:

571   SAMN11351981, SAMN11351982, SAMN11351983, SAMN11351984, SAMN00188192,

572   SAMN00188193; Sleeping Beauty: SAMN02870102; and PiggyBac: SAMN02870101) and

573   computationally mapped and analyzed in the same manner as the in-house generated data using

574   Python (v3.7.10, run on CentOS 7 Linux).

575   *In vivo* **study design**

576   Specific pathogen-free female NOD-scid IL2Rgammanull (NSG) mice were purchased from The

577   Jackson Laboratory (RRID:IMSR_JAX:005557). Tumor challenge studies were performed using

578   the Raji-luc CD155hi/PD-L1hi cell line. Specifically, mice were implanted with 1E5 Raji cells

579   resuspended in PBS and delivered in 100 µL via tail vein. Two days post tumor implantation, the

580   mice were randomized into treatment groups (n=5) and received either PBS, non-engineered

581   (control) NK cells, CAR NK cells, CAR15 NK cells, CTP^{KO} NK cells, CAR/CTP^{KO} NK cells, or

582   CAR15/CTP^{KO} NK cells the next day. For each group, all tumor growth was monitored by weekly

583   bioluminescence imaging of mice 5 minutes post IP injection of D-luciferin (100 µL total volume,

584   28 mg/kg) using an IVIS® Spectrum *in vivo* imaging system followed by ROI analysis of tumor

585   images (Living Image software, version 4.7.3). NK cell persistence in peripheral blood was

586   monitored by weekly submandibular blood collection. Endpoint criteria are either mouse paralysis

587   or >20% weight loss within a week. At endpoint, peripheral blood, spleen, and bone marrow were

588   collected and processed to single cell suspensions through standard mashing and ACK-processing

589   and stained for phenotyping markers. This study was carried out in strict accordance with the

590   recommendations in the Guide for the Care and Use of Laboratory Animals of the National

591   Institutes of Health. The protocol and all procedures were approved by the University of Minnesota

592   Institutional Animal Care and Use Committee (Protocol #2110-39527A). The health of the mice

593   was monitored daily by University of Minnesota veterinary staff.

594   **Statistical analysis**

595   The Student's t-test was used to evaluate the significance of differences between the two groups.

596   Differences between three or more groups with one data point were evaluated by a one-way

597   ANOVA test. Differences between three or more groups with multiple data points were evaluated

598   by a two-way ANOVA test. Differences between groups in our *in vivo* study were evaluated by

599   the Log-rank (Mantel-Cox) test. The level of significance was set at α = 0.05. All statistical

600   analyses were performed using GraphPad Prism 9.2.0.

Conflict of interest statement

M.W., E.J.P., M.G.K., B.S.M. and B.R.W. have filed patents covering the methods and approaches outlined in this work.

References

1. Ruggeri, L. *et al.* Effectiveness of donor natural killer cell alloreactivity in mismatched hematopoietic transplants. *Science* **295**, 2097–2100 (2002).

2. Pan, K. *et al.* CAR race to cancer immunotherapy: from CAR T, CAR NK to CAR macrophage therapy. *J. Exp. Clin. Cancer Res.* **41**, 119 (2022).

3. Suck, G. *et al.* NK-92: an 'off-the-shelf therapeutic' for adoptive natural killer cell-based cancer immunotherapy. *Cancer Immunol. Immunother.* **65**, 485–492 (2016).

4. Miller, J. S. & Lanier, L. L. Natural Killer Cells in Cancer Immunotherapy. *Annu. Rev. Cancer Biol.* **3**, 77–103 (2019).

5. Judge, S. J., Murphy, W. J. & Canter, R. J. Characterizing the Dysfunctional NK Cell: Assessing the Clinical Relevance of Exhaustion, Anergy, and Senescence. *Front. Cell. Infect. Microbiol.* **10**, 49 (2020).

6. Gong, Y., Klein Wolterink, R. G. J., Wang, J., Bos, G. M. J. & Germeraad, W. T. V. Chimeric antigen receptor natural killer (CAR-NK) cell design and engineering for cancer therapy. *J. Hematol. Oncol.* **14**, 73 (2021).

7. Gurney, M. *et al.* Concurrent transposon engineering and CRISPR/Cas9 genome editing of primary CLL-1 chimeric antigen receptor-natural killer cells. *Cytotherapy* **24**, 1087–1094 (2022).

8. Ma, S., Caligiuri, M. A. & Yu, J. Harnessing IL-15 signaling to potentiate NK cell-mediated cancer immunotherapy. *Trends Immunol.* **43**, 833–847 (2022).

9. Rosenberg, S. A. *et al.* Observations on the systemic administration of autologous lymphokine-activated killer cells and recombinant interleukin-2 to patients with metastatic cancer. *N. Engl. J. Med.* **313**, 1485–1492 (1985).

637   10. Rosenberg, S. A. The development of new immunotherapies for the treatment of cancer

638   using interleukin-2. A review. *Ann. Surg.* **208**, 121–135 (1988).

639   11. Lodolce, J. P., Burkett, P. R., Koka, R. M., Boone, D. L. & Ma, A. Regulation of lymphoid

640   homeostasis by interleukin-15. *Cytokine Growth Factor Rev.* **13**, 429–439 (2002).

641   12. Suck, G. & Koh, M. B. C. Emerging natural killer cell immunotherapies: large-scale ex vivo

642   production of highly potent anticancer effectors. *Hematol. Oncol. Stem Cell Ther.* **3**, 135–

643   142 (2010).

644   13. Suck, G. *et al.* Interleukin-15 supports generation of highly potent clinical-grade natural

645   killer cells in long-term cultures for targeting hematological malignancies. *Exp. Hematol.*

646   **39**, 904–914 (2011).

647   14. Conlon, K. C. *et al.* Redistribution, hyperproliferation, activation of natural killer cells and

648   CD8 T cells, and cytokine production during first-in-human clinical trial of recombinant

649   human interleukin-15 in patients with cancer. *J. Clin. Oncol.* **33**, 74–82 (2015).

650   15. Waldmann, T. A., Dubois, S., Miljkovic, M. D. & Conlon, K. C. IL-15 in the Combination

651   Immunotherapy of Cancer. *Front. Immunol.* **11**, 868 (2020).

652   16. Zhou, Y. *et al.* Interleukin 15 in Cell-Based Cancer Immunotherapy. *Int. J. Mol. Sci.* **23**,

653   (2022).

654   17. Christodoulou, I. *et al.* Engineering CAR-NK cells to secrete IL-15 sustains their anti-AML

655   functionality but is associated with systemic toxicities. *J Immunother Cancer* **9**, (2021).

656   18. Liu, E. *et al.* Use of CAR-Transduced Natural Killer Cells in CD19-Positive Lymphoid

657   Tumors. *N. Engl. J. Med.* **382**, 545–553 (2020).

658   19. Liu, E. *et al.* Cord blood NK cells engineered to express IL-15 and a CD19-targeted CAR

659   show long-term persistence and potent antitumor activity. *Leukemia* **32**, 520–531 (2018).

660   20. Pomeroy, E. J. *et al.* A Genetically Engineered Primary Human Natural Killer Cell Platform

661   for Cancer Immunotherapy. *Mol. Ther.* **28**, 52–63 (2020).

662   21. Naeimi Kararoudi, M. *et al.* Generation of Knock-out Primary and Expanded Human NK

663   Cells Using Cas9 Ribonucleoproteins. *J. Vis. Exp.* (2018) doi:10.3791/58237.

664   22. Bexte, T. *et al.* CRISPR-Cas9 based gene editing of the immune checkpoint NKG2A

665   enhances NK cell mediated cytotoxicity against multiple myeloma. *Oncoimmunology* **11**,

666   2081415 (2022).

667   23. Mohammadian Gol, T. *et al.* CRISPR-Cas9-Based Gene Knockout of Immune Checkpoints

668   in Expanded NK Cells. *Int. J. Mol. Sci.* **24**, (2023).

669   24. Nakazawa, T. *et al.* CIS deletion by CRISPR/Cas9 enhances human primary natural killer

670   cell functions against allogeneic glioblastoma. *J. Exp. Clin. Cancer Res.* **42**, 205 (2023).

671   25. Webber, B. R. *et al.* Highly efficient multiplex human T cell engineering without double-

672   strand breaks using Cas9 base editors. *Nat. Commun.* **10**, 5222 (2019).

673   26. Komor, A. C., Kim, Y. B., Packer, M. S., Zuris, J. A. & Liu, D. R. Programmable editing of

674   a target base in genomic DNA without double-stranded DNA cleavage. *Nature* **533**, 420–

675   424 (2016).

676   27. Gaudelli, N. M. *et al.* Programmable base editing of A•T to G•C in genomic DNA without

677   DNA cleavage. *Nature* **551**, 464–471 (2017).

678   28. Rees, H. A. & Liu, D. R. Base editing: precision chemistry on the genome and

679   transcriptome of living cells. *Nat. Rev. Genet.* **19**, 770–788 (2018).

680   29. Kantor, A., McClements, M. E. & MacLaren, R. E. CRISPR-Cas9 DNA Base-Editing and

681   Prime-Editing. *Int. J. Mol. Sci.* **21**, (2020).

682   30. Richter, M. F. *et al.* Phage-assisted evolution of an adenine base editor with improved Cas

683   domain compatibility and activity. *Nat. Biotechnol.* **38**, 883–891 (2020).

684 31. Liu, X. *et al.* CRISPR-Cas9-mediated multiplex gene editing in CAR-T cells. *Cell Res.* **27**,

685   154–157 (2017).

686 32. Kuscu, C. *et al.* CRISPR-STOP: gene silencing through base-editing-induced nonsense

687   mutations. *Nat. Methods* **14**, 710–712 (2017).

688 33. Dang, L. *et al.* Comparison of gene disruption induced by cytosine base editing-mediated

689   iSTOP with CRISPR/Cas9-mediated frameshift. *Cell Prolif.* **53**, e12820 (2020).

690 34. Zhu, H. *et al.* Metabolic Reprograming via Deletion of CISH in Human iPSC-Derived NK

691   Cells Promotes In Vivo Persistence and Enhances Anti-tumor Activity. *Cell Stem Cell* **27**,

692   224–237.e6 (2020).

693 35. Kluesner, M. G. *et al.* CRISPR-Cas9 cytidine and adenosine base editing of splice-sites

694   mediates highly-efficient disruption of proteins in primary and immortalized cells. *Nat.*

695   *Commun.* **12**, 2437 (2021).

696 36. Myers, J. A. & Miller, J. S. Exploring the NK cell platform for cancer immunotherapy. *Nat.*

697   *Rev. Clin. Oncol.* **18**, 85–100 (2021).

698 37. Trikha, P. *et al.* Defining the AHR-regulated transcriptome in NK cells reveals gene

699   expression programs relevant to development and function. *Blood Adv* **5**, 4605–4618

700   (2021).

701 38. Bai, R. & Cui, J. Burgeoning Exploration of the Role of Natural Killer Cells in Anti-PD-

702   1/PD-L1 Therapy. *Front. Immunol.* **13**, 886931 (2022).

703 39. Rousseau, A., Parisi, C. & Barlesi, F. Anti-TIGIT therapies for solid tumors: a systematic

704   review. *ESMO Open* **8**, 101184 (2023).

705 40. Saito, M. *et al.* KLMab-1: An Anti-human KLRG1 Monoclonal Antibody for

706   Immunocytochemistry. *Monoclon. Antib. Immunodiagn. Immunother.* **41**, 279–284 (2022).

707   41. Kluesner, M. G. *et al.* EditR: A Method to Quantify Base Editing from Sanger Sequencing.

708   *CRISPR J* **1**, 239–250 (2018).

709   42. Benson, D. M., Jr *et al.* The PD-1/PD-L1 axis modulates the natural killer cell versus

710   multiple myeloma effect: a therapeutic target for CT-011, a novel monoclonal anti-PD-1

711   antibody. *Blood* **116**, 2286–2294 (2010).

712   43. MacFarlane, A. W., 4th *et al.* PD-1 expression on peripheral blood cells increases with

713   stage in renal cell carcinoma patients and is rapidly reduced after surgical tumor resection.

714   *Cancer Immunol Res* **2**, 320–331 (2014).

715   44. Beldi-Ferchiou, A. *et al.* PD-1 mediates functional exhaustion of activated NK cells in

716   patients with Kaposi sarcoma. *Oncotarget* **7**, 72961–72977 (2016).

717   45. Liu, Y. *et al.* Increased expression of programmed cell death protein 1 on NK cells inhibits

718   NK-cell-mediated anti-tumor function and indicates poor prognosis in digestive cancers.

719   *Oncogene* **36**, 6143–6153 (2017).

720   46. Pesce, S. *et al.* Identification of a subset of human natural killer cells expressing high levels

721   of programmed death 1: A phenotypic and functional characterization. *J. Allergy Clin.*

722   *Immunol.* **139**, 335–346.e3 (2017).

723   47. Vari, F. *et al.* Immune evasion via PD-1/PD-L1 on NK cells and monocyte/macrophages is

724   more prominent in Hodgkin lymphoma than DLBCL. *Blood* **131**, 1809–1819 (2018).

725   48. Tumino, N. *et al.* Presence of innate lymphoid cells in pleural effusions of primary and

726   metastatic tumors: Functional analysis and expression of PD-1 receptor. *Int. J. Cancer* **145**,

727   1660–1668 (2019).

728   49. Pesce, S. *et al.* Different Features of Tumor-Associated NK Cells in Patients With Low-

729   Grade or High-Grade Peritoneal Carcinomatosis. *Front. Immunol.* **10**, 1963 (2019).

730   50. Quatrini, L. *et al.* The Immune Checkpoint PD-1 in Natural Killer Cells: Expression,

731   Function and Targeting in Tumour Immunotherapy. *Cancers* **12**, (2020).

732   51. Opitz, C. A. *et al.* An endogenous tumour-promoting ligand of the human aryl hydrocarbon

733   receptor. *Nature* **478**, 197–203 (2011).

734   52. Bernard, P.-L. *et al.* Targeting CISH enhances natural cytotoxicity receptor signaling and

735   reduces NK cell exhaustion to improve solid tumor immunity. *J Immunother Cancer* **10**,

736   (2022).

737   53. Yusubalieva, G. M. *et al.* [Enhanced Natural Killers with CISH and B2M Gene Knockouts

738   Reveal Increased Cytotoxicity in Glioblastoma Primary Cultures]. *Mol. Biol.* **56**, 848–859

739   (2022).

740   54. Sarhan, D. *et al.* Adaptive NK Cells with Low TIGIT Expression Are Inherently Resistant

741   to Myeloid-Derived Suppressor Cells. *Cancer Res.* **76**, 5696–5706 (2016).

742   55. Rishiq, A., Bsoul, R., Pick, O. & Mandelboim, O. Studying TIGIT activity against tumors

743   through the generation of knockout mice. *Oncoimmunology* **12**, 2217735 (2023).

744   56. Hasan, M. F. *et al.* Knockout of the inhibitory receptor TIGIT enhances the antitumor

745   response of ex vivo expanded NK cells and prevents fratricide with therapeutic Fc-active

746   TIGIT antibodies. *J Immunother Cancer* **11**, (2023).

747   57. Hsu, J. *et al.* Contribution of NK cells to immunotherapy mediated by PD-1/PD-L1

748   blockade. *J. Clin. Invest.* **128**, 4654–4668 (2018).

749   58. Pesce, S. *et al.* PD/1-PD-Ls Checkpoint: Insight on the Potential Role of NK Cells. *Front.*

750   *Immunol.* **10**, 1242 (2019).

751   59. Sivori, S. *et al.* Human NK cells: surface receptors, inhibitory checkpoints, and translational

752   applications. *Cell. Mol. Immunol.* **16**, 430–441 (2019).

753   60. Khan, M., Arooj, S. & Wang, H. NK Cell-Based Immune Checkpoint Inhibition. *Front.*

754   *Immunol.* **11**, 167 (2020).

755   61. Ito, M. *et al.* Killer cell lectin-like receptor G1 binds three members of the classical

756   cadherin family to inhibit NK cell cytotoxicity. *J. Exp. Med.* **203**, 289–295 (2006).

757   62. Dixon, K. J., Wu, J. & Walcheck, B. Engineering Anti-Tumor Monoclonal Antibodies and

758   Fc Receptors to Enhance ADCC by Human NK Cells. *Cancers* **13**, (2021).

759   63. Wu, J., Mishra, H. K. & Walcheck, B. Role of ADAM17 as a regulatory checkpoint of

760   CD16A in NK cells and as a potential target for cancer immunotherapy. *J. Leukoc. Biol.*

761   **105**, 1297–1303 (2019).

762   64. Jing, Y. *et al.* Identification of an ADAM17 cleavage region in human CD16 (FcγRIII) and

763   the engineering of a non-cleavable version of the receptor in NK cells. *PLoS One* **10**,

764   e0121788 (2015).

765   65. Nakano, O. *et al.* Proliferative activity of intratumoral CD8(+) T-lymphocytes as a

766   prognostic factor in human renal cell carcinoma: clinicopathologic demonstration of

767   antitumor immunity. *Cancer Res.* **61**, 5132–5136 (2001).

768   66. Ghebeh, H. *et al.* The B7-H1 (PD-L1) T lymphocyte-inhibitory molecule is expressed in

769   breast cancer patients with infiltrating ductal carcinoma: correlation with important high-

770   risk prognostic factors. *Neoplasia* **8**, 190–198 (2006).

771   67. Abiko, K. *et al.* PD-L1 on tumor cells is induced in ascites and promotes peritoneal

772   dissemination of ovarian cancer through CTL dysfunction. *Clin. Cancer Res.* **19**, 1363–

773   1374 (2013).

774   68. Yang, C.-Y., Lin, M.-W., Chang, Y.-L., Wu, C.-T. & Yang, P.-C. Programmed cell death-

775   ligand 1 expression is associated with a favourable immune microenvironment and better

776   overall survival in stage I pulmonary squamous cell carcinoma. *Eur. J. Cancer* **57**, 91–103

777   (2016).

778   69. Yeo, M.-K. *et al.* Association of PD-L1 expression and PD-L1 gene polymorphism with

779   poor prognosis in lung adenocarcinoma and squamous cell carcinoma. *Hum. Pathol.* **68**,

780   103–111 (2017).

781   70. Zhao, Y. *et al.* Prognostic significance of PD-L1 in advanced non-small cell lung

782   carcinoma. *Medicine* **99**, e23172 (2020).

783   71. Oyama, R. *et al.* CD155 expression and its clinical significance in non-small cell lung

784   cancer. *Oncol. Lett.* **23**, 166 (2022).

785   72. Zhang, D., Liu, J., Zheng, M., Meng, C. & Liao, J. Prognostic and clinicopathological

786   significance of CD155 expression in cancer patients: a meta-analysis. *World J. Surg. Oncol.*

787   **20**, 351 (2022).

788   73. Murakami, D. *et al.* Prognostic value of CD155/TIGIT expression in patients with

789   colorectal cancer. *PLoS One* **17**, e0265908 (2022).

790   74. Rafei, H., Daher, M. & Rezvani, K. Chimeric antigen receptor (CAR) natural killer (NK)-

791   cell therapy: leveraging the power of innate immunity. *Br. J. Haematol.* **193**, 216–230

792   (2021).

793   75. Guven, H. *et al.* Efficient gene transfer into primary human natural killer cells by retroviral

794   transduction. *Exp. Hematol.* **33**, 1320–1328 (2005).

795   76. Streltsova, M. A., Barsov, E., Erokhina, S. A. & Kovalenko, E. I. Retroviral gene transfer

796   into primary human NK cells activated by IL-2 and K562 feeder cells expressing

797   membrane-bound IL-21. *J. Immunol. Methods* **450**, 90–94 (2017).

798   77. Xie, G. *et al.* CAR-NK cells: A promising cellular immunotherapy for cancer.

799   *EBioMedicine* **59**, 102975 (2020).

800   78. Obreht, I. *et al.* Shift of large-scale atmospheric systems over Europe during late MIS 3 and

801   implications for Modern Human dispersal. *Sci. Rep.* **7**, 5848 (2017).

802   79. Li, L. *et al.* Loss of metabolic fitness drives tumor resistance after CAR-NK cell therapy

803   and can be overcome by cytokine engineering. *Sci Adv* **9**, eadd6997 (2023).

804   80. Philip, B. *et al.* A highly compact epitope-based marker/suicide gene for easier and safer T-

805   cell therapy. *Blood* **124**, 1277–1287 (2014).

806   81. Elmas, E. *et al.* CRISPR Gene Editing of Human Primary NK and T Cells for Cancer

807   Immunotherapy. *Front. Oncol.* **12**, 834002 (2022).

808   82. Naeimi Kararoudi, M. *et al.* Optimization and validation of CAR transduction into human

809   primary NK cells using CRISPR and AAV. *Cell Rep Methods* **2**, 100236 (2022).

810   83. Huang, R.-S., Shih, H.-A., Lai, M.-C., Chang, Y.-J. & Lin, S. Enhanced NK-92

811   Cytotoxicity by CRISPR Genome Engineering Using Cas9 Ribonucleoproteins. *Front.*

812   *Immunol.* **11**, 1008 (2020).

813   84. Gründemann, C. *et al.* The NK receptor KLRG1 is dispensable for virus-induced NK and

814   CD8+ T-cell differentiation and function in vivo. *Eur. J. Immunol.* **40**, 1303–1314 (2010).

815   85. Jonjic, S. Functional plasticity and robustness are essential characteristics of biological

816   systems: lessons learned from KLRG1-deficient mice. *Eur. J. Immunol.* **40**, 1241–1243

817   (2010).

818   86. Mariotti, F. R. *et al.* PD-1 in human NK cells: evidence of cytoplasmic mRNA and protein

819   expression. *Oncoimmunology* **8**, 1557030 (2019).

820   87. Davis, Z. *et al.* Low-density PD-1 expression on resting human natural killer cells is

821   functional and upregulated after transplantation. *Blood Adv* **5**, 1069–1080 (2021).

822   88.   Lai, P. *et al.* Alterations in expression and function of signal-transducing proteins in tumor-

823   associated T and natural killer cells in patients with ovarian carcinoma. *Clin. Cancer Res.* **2**,

824   161–173 (1996).

825   89.   Jewett, A. & Tseng, H.-C. Tumor induced inactivation of natural killer cell cytotoxic

826   function; implication in growth, expansion and differentiation of cancer stem cells. *J.*

827   *Cancer* **2**, 443–457 (2011).

828   90.   Tachibana, R. *et al.* Quantitative analysis of correlation between number of nuclear

829   plasmids and gene expression activity after transfection with cationic liposomes. *Pharm.*

830   *Res.* **19**, 377–381 (2002).

831   91.   Glover, D. J., Leyton, D. L., Moseley, G. W. & Jans, D. A. The efficiency of nuclear

832   plasmid DNA delivery is a critical determinant of transgene expression at the single cell

833   level. *J. Gene Med.* **12**, 77–85 (2010).

834   92.   Colamartino, A. B. L. *et al.* Efficient and Robust NK-Cell Transduction With Baboon

835   Envelope Pseudotyped Lentivector. *Front. Immunol.* **10**, 2873 (2019).

836   93.   Pogue, A. I., Jaber, V., Zhao, Y. & Lukiw, W. J. Systemic Inflammation in C57BL/6J Mice

837   Receiving Dietary Aluminum Sulfate; Up-Regulation of the Pro-Inflammatory Cytokines

838   IL-6 and TNFα, C-Reactive Protein (CRP) and miRNA-146a in Blood Serum. *J. Alzheimers*

839   *Dis. Parkinsonism* **7**, (2017).

840   94.   Newell, M. K., Villalobos-Menuey, E., Schweitzer, S. C., Harper, M.-E. & Camley, R. E.

841   Cellular metabolism as a basis for immune privilege. *J. Immune Based Ther. Vaccines* **4**, 1

842   (2006).

843   95.   Wong, D. P. *et al.* A BAFF ligand-based CAR-T cell targeting three receptors and multiple

844   B cell cancers. *Nat. Commun.* **13**, 217 (2022).

845 96. Delconte, R. B. *et al.* CIS is a potent checkpoint in NK cell-mediated tumor immunity. *Nat.*

846   *Immunol.* **17**, 816–824 (2016).

847 97. Zhang, Q. *et al.* Blockade of the checkpoint receptor TIGIT prevents NK cell exhaustion

848   and elicits potent anti-tumor immunity. *Nat. Immunol.* **19**, 723–732 (2018).

849 98. Tata, A. *et al.* Combination blockade of KLRG1 and PD-1 promotes immune control of

850   local and disseminated cancers. *Oncoimmunology* **10**, 1933808 (2021).

1 **Table 1 List of genes for KO in NK cells using BE.**

Gene Name	Protein Name	Subcellular Location	Functions in NK Cell	sgRNA Sequence
AHR	Aryl hydrocarbon receptor (AhR)	Intracellular	Positive regulator of CD56 expression in NK cells[37]	CTT**A**CCATCAAAGAAGCTCT
CISH	Cytokine-inducible SH2-containing protein (CIS)	Intracellular	Negative regulator of IL-15 signaling in NK cells[96]	CTC**A**CCAGATTCCCGAAGGT
TIGIT	T cell immunoreceptor with Ig and ITIM domains	Cell Membrane	Immune checkpoint in NK cells leads to cell exhaustion[97]	CAGGCCTT**A**CCTGAGGCGAG
KLRG1	Killer cell lectin-like receptor subfamily G member 1	Cell Membrane	Inhibitory receptor on NK cell surfaces[98]	CCTT**A**CCTTGAGAAGTTTAG
PDCD1	Programmed cell death protein 1 (PD-1/CD279)	Cell Membrane	Immune checkpoint in NK cells that plays a role in immunosuppression[58]	CACCT**A**CCTAAGAACCATCC

2
3
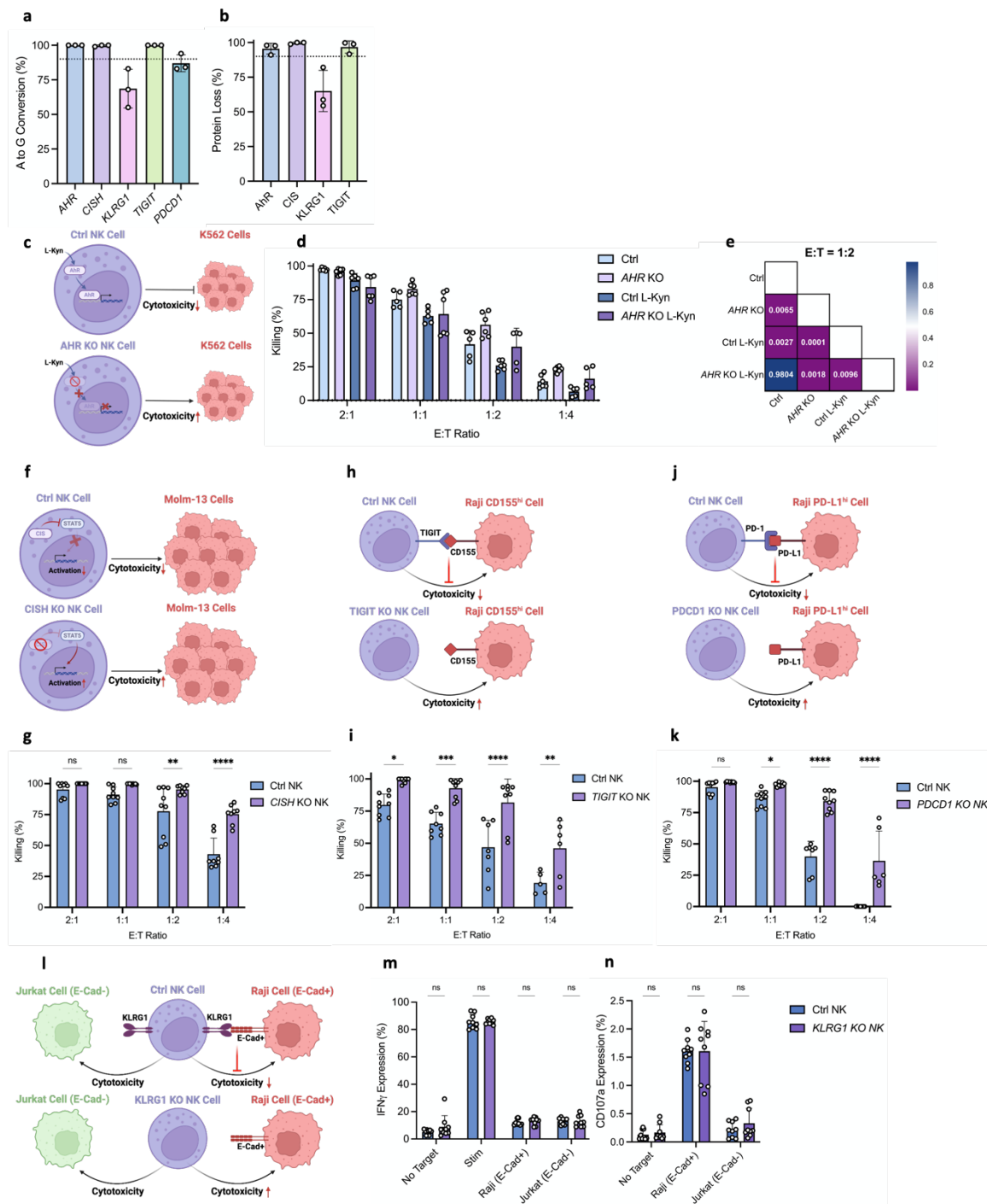
Fig. 1 Highly efficient single gene KO in NK cells using BE. a Editing efficiency at genomic level quantified by A to G conversion of target base for each gene locus (n=3 independent NK cell donors). **b** Editing efficiency at protein level quantified by percentage of protein loss of each gene (n=3 independent NK cell donors). **c** Schema of killing assay to assess the functional improvement

9   of AHR KO NK cells. **d** Ability of AHR KO versus Ctrl NK cells (with or without 14 days of L-

10   Kynurenine pre-treatment) to kill K562 cells at various E:T ratios as measured by luciferase

11   luminescence assay. Assays run in triplicate in n=2 independent biological NK cell donors. **e**

12   Statistical significance (P-value) between each condition of AHR KO functional killing assay at E

13   to T ratio of 1:2. **f** Schema of killing assay to assess the functional improvement of CISH KO NK

14   cells. **g** Ability of CISH KO versus Ctrl NK cells to kill Molm-13 cells at various E:T ratios as

15   measured by luciferase luminescence assay. Assays run in triplicate in n=3 independent biological

16   NK cell donors. **h** Schema of killing assay to assess the functional improvement of TIGIT KO NK

17   cells. **i** Ability of TIGIT KO versus Ctrl NK cells to kill Raji CD155^{hi} cells at various E:T ratios

18   as measured by luciferase luminescence assay. Assays run in triplicate in n=3 independent

19   biological NK cell donors. **j** Schema of killing assay to assess the functional improvement of

20   PDCD1 KO NK cells. **k** Ability of PDCD1 KO versus Ctrl NK cells to kill Raji PD-L1^{hi} cells at

21   various E:T ratios as measured by luciferase luminescence assay. Assays run in triplicate in n=3

22   independent biological NK cell donors. **l** Schema of ICS assay to assess the functional

23   improvement of KLRG1 KO NK cells. **m&n** Cytokine production (**m**) and degranulation (**n**)

24   ability of KLRG1 KO versus Ctrl NK cells against E-Cad+ Raji cells or E-Cad- Jurkat cells as

25   measured by percentage of NK cells produce IFNγ and CD107a. Assays run in triplicate in n=3

26   independent biological NK cell donors. Data represented as mean ± SD. P-values calculated by

27   two-way ANOVA test (n.s.P > 0.05, *P ≤ 0.05, **P ≤ 0.01, ***P ≤ 0.001, ****P ≤ 0.0001).

28

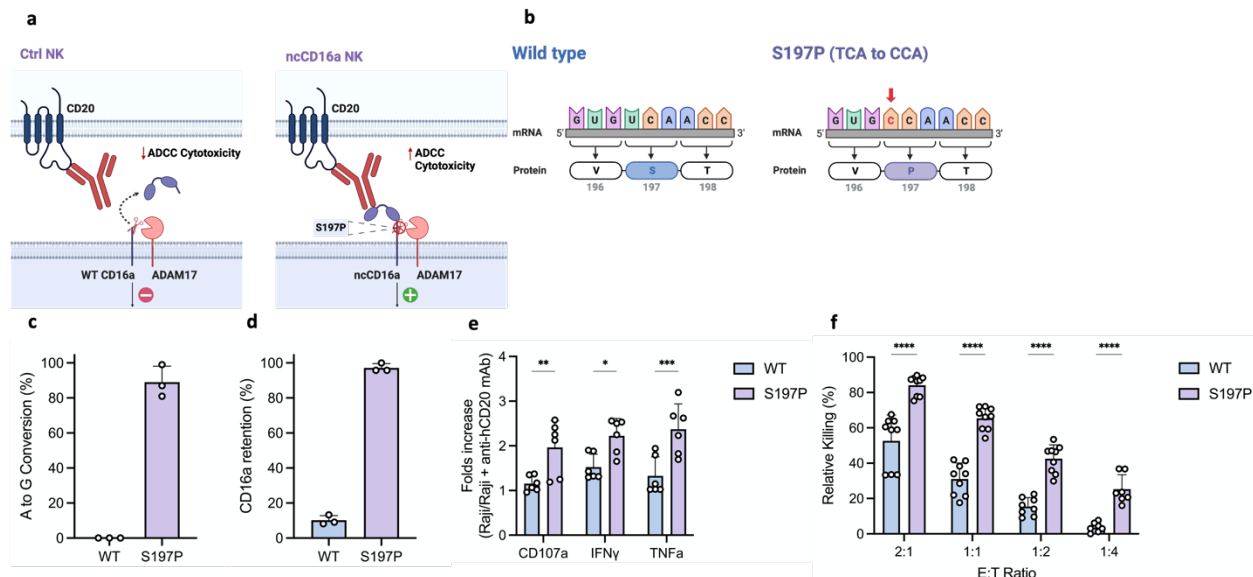**Fig. 2 Highly efficient gain-of-function mutation in NK cells using BE. a** Schema of how the S197P mutation renders NK cells non-cleavable by ADAM17 and results in enhanced ADCC cytotoxicity. **b** Schema of the recreation of S197P ncCD16a NK cells by a single base modification by BE. **c** Editing efficiency at genomic level quantified by A to G conversion of target base for *CD16A* (n=3 independent NK cell donors). **d** Editing efficiency at protein level quantified by CD16a retention on NK cell surface after PMA treatment (n=3 independent NK cell donors). **e** Cytokine production of S197P CD16a versus WT CD16a NK cells against CD20+ Raji cells during ADCC (E:T ratio: 1:1). Plotted by folds increase of each cytokine with versus without anti-hCD20 mAb co-treatment. Assays run in duplicate in n=3 independent biological NK cell donors. **f** Ability of S197P CD16a versus WT CD16a NK cells to carry out ADCC against anti-hCD20 mAb treated CD20+ Raji cells at various E:T ratios as measured by luciferase luminescence assay. Assays run in triplicate in n=3 independent biological NK cell donors. Data represented as mean ± SD. P-values calculated by two-way ANOVA test (*P ≤ 0.05, **P ≤ 0.01, ***P ≤ 0.001, ****P ≤ 0.0001)
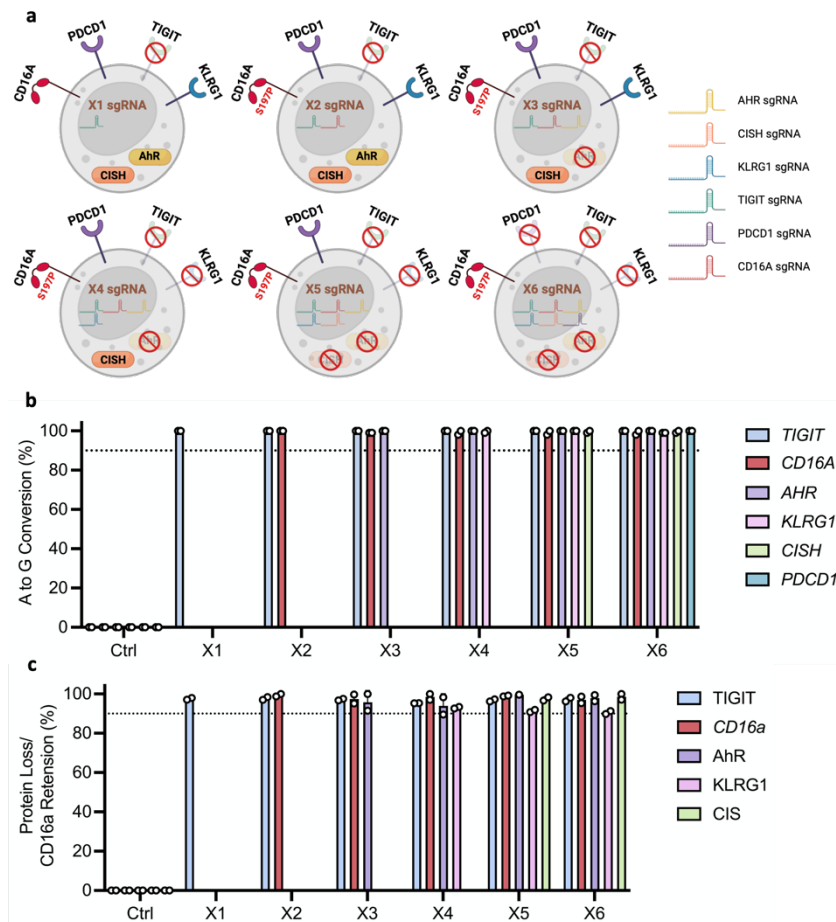
Fig. 3 Highly efficient multiplex editing in NK cells using BE. a Schema of multiplex editing strategy. **b** Multiplex editing efficiency at genomic level quantified by A to G conversion of target base for each gene locus (n=2 independent NK cell donors). **c** Multiplex editing efficiency at protein level quantified by percentage of protein loss of each gene (n=2 independent NK cell donors). Data represented as mean ± SD.
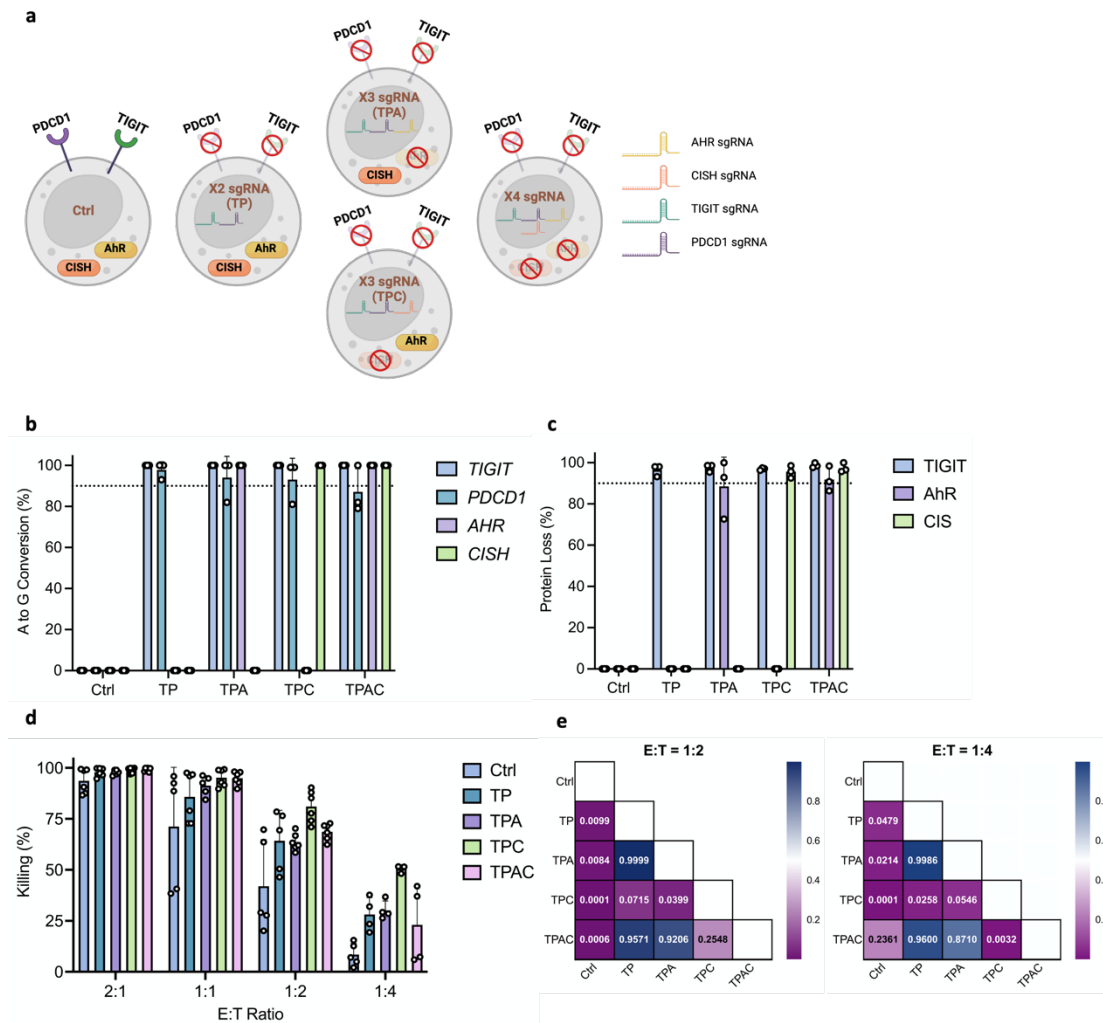
Fig. 4 Optimization of multiplex KO to maximize NK functionality against Raji$^{hi/hi}$. a Schema of optimization strategy and all possible KO combinations included. **b** Editing efficiency at genomic level quantified by A to G conversion of target base for each gene locus (n=3 independent NK cell donors). **c** Editing efficiency at protein level quantified by percentage of protein loss of each gene (n=3 independent NK cell donors). **d** Ability of each KO combination to kill Raji$^{hi/hi}$ cells at various E:T ratios as measured by luciferase luminescence assay. Assays run in triplicate in n=2 independent biological NK cell donors. **e** Functional killing assay statistical significance (P-value) between each KO combination at E to T ratio of 1:2 and 1:4. Ctrl: ABE8e mRNA only, TP: *TIGIT* and *PDCD1* KO, TPA: *TIGIT*, *PDCD1*, and *AHR* KO, TPC: *TIGIT*, *PDCD1*, and *CISH*

62   KO, TPAC: *TIGIT*, *PDCD1*, *AHR,* and *CISH* KO. Data represented as mean ± SD. P-values
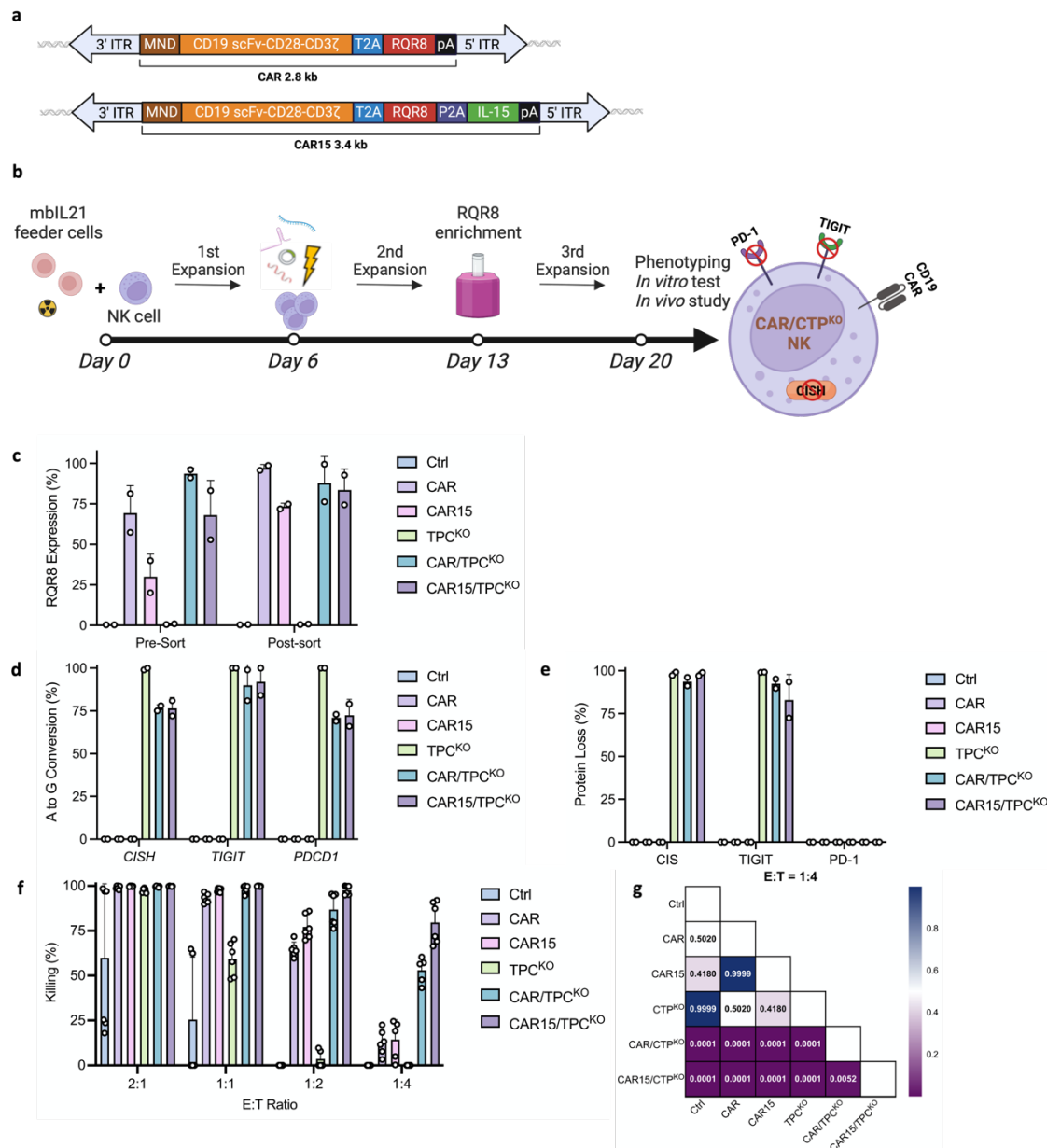
63   calculated by two-way ANOVA test.

64

Fig. 5 Simultaneous BE and non-viral transposon engineering exhibited enhanced NK cytotoxicity. a Schema of the designs of CD19 CAR constructs. **b** Schema of NK cell engineering timeline for simultaneous sgRNAs and CD19 CAR delivery. **c** Pre-sorting and post-sorting CAR integration rate quantified by percentage of RQR8 expression on NK cells (n=2 independent NK cell donors). **d** Post-sorting editing efficiency at genomic level quantified by A to G conversion of target base for each gene locus (n=2 independent NK cell donors). **e** Post-sorting editing efficiency

72 at protein level quantified by percentage of protein loss of each gene (n=2 independent NK cell

73 donors). **f** *In vitro* testing of the cytotoxicity of simultaneous BE and TcBuster engineered NK

74 cells against Raji^{hi/hi} cells at various E:T ratios as measured by luciferase luminescence assay.

75 Assays run in triplicate in n=2 independent biological NK cell donors. **g** Killing assay statistical

76 significance (P-value) between each condition at E to T ratio of 1:4. Ctrl: ABE8e mRNA and CAR-

77 expressing nanoplasmid only, CAR: CD19 CAR RQR8; CAR15: CD19 CAR RQR8 IL-15; CTP^{KO}:

78 *CISH*, *TIGIT*, and *PDCD1* KO; CAR/CTP^{KO}: CD19 CAR RQR8 with *CISH*, *TIGIT*, and *PDCD1*

79 KO; CAR15/CTP^{KO}: CD19 CAR RQR8 IL-15 with *CISH*, *TIGIT*, and *PDCD1* KO. Data

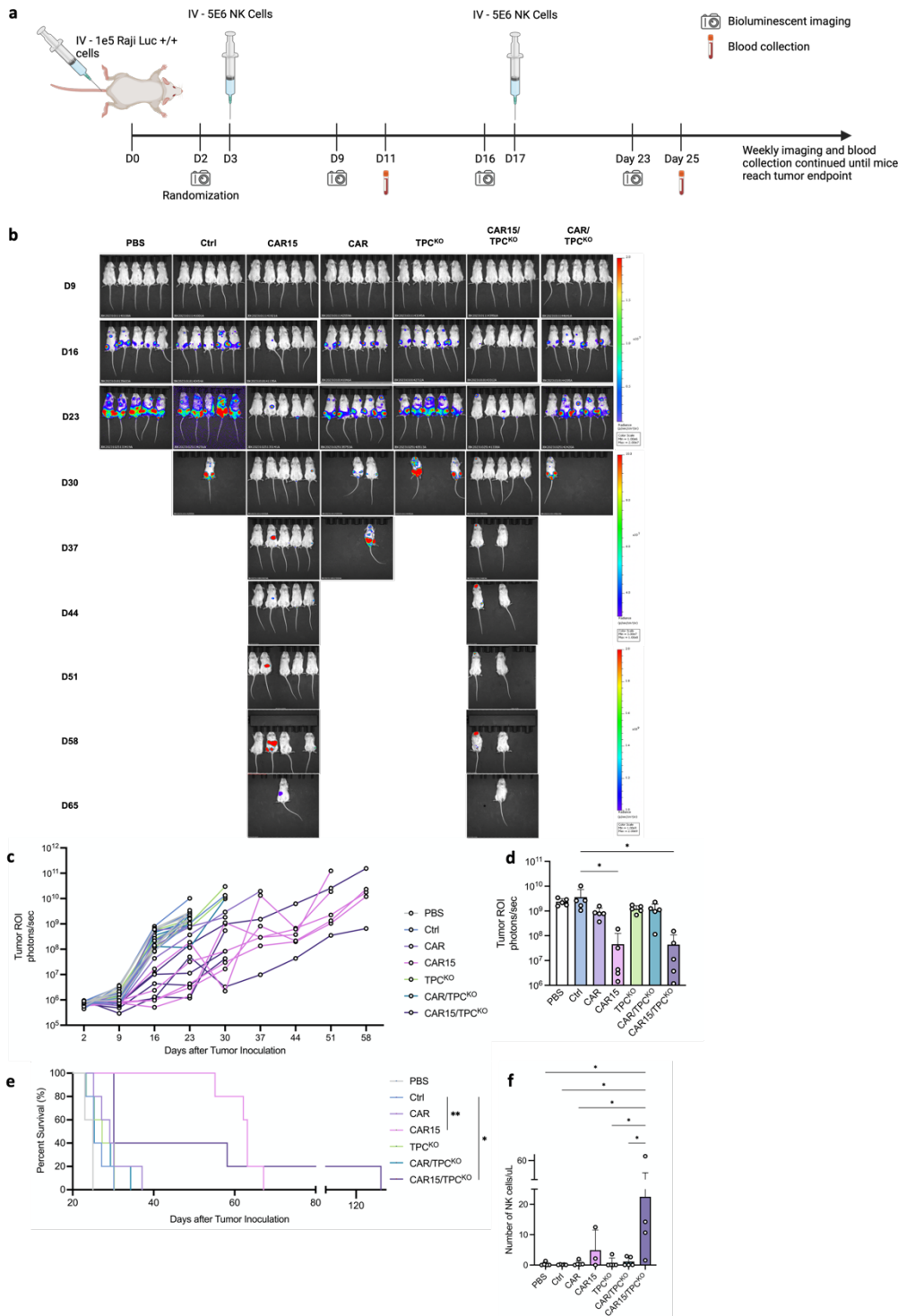80 represented as mean ± SD. P-values calculated by two-way ANOVA test.

81

Fig. 6 Multiplex edited CD19 CAR-NK cells are highly functional *in vivo*. a Schema of *in vivo* study design and timeline. **b-c** Luminance (ROI) of individual tumor burden of mice bearing Raji[hi/hi] cells following treatment with PBS, Ctrl or engineered NK cells. **d** Tumor burden of each

86   group on day 23, quantified by ROI (photons/sec) of each mouse (n=5). P-values calculated by

87   one-way ANOVA test (*P ≤ 0.05). **e** Survival curve of each group shown in Kaplan-Meier curve

88   (n=5). P-values calculated by Mantel-Cox test. Ctrl versus CAR15, **P ≤ 0.01; Ctrl versus

89   CAR15/CTP^{KO}, *P ≤ 0.05. **f** Numbers of circulating NK cells measured by NK cell number per

90   uL of peripheral blood at end point. Data represented as mean ± SD.

91

92